

PROCEEDINGS OF SPIE

[SPIDigitalLibrary.org/conference-proceedings-of-spie](https://spiedigitallibrary.org/conference-proceedings-of-spie)

Testing of a germanium immersion grating

Matthew J. Richter, Peter T. Zell, Jeffrey S. Logan, Robert E. McMurray, Curtis N. DeWitt, et al.

Matthew J. Richter, Peter T. Zell, Jeffrey S. Logan, Robert E. McMurray, Curtis N. DeWitt, Karl W. Kaess, Isaiah B. Santistevan, Edward J. Montiel, Adwin Boogert, Thomas P. Greene, Scott A. Sandford, Takashi Sukagawa, Paul J. Kuzmenko, "Testing of a germanium immersion grating," Proc. SPIE 10706, Advances in Optical and Mechanical Technologies for Telescopes and Instrumentation III, 1070652 (10 July 2018); doi: 10.1117/12.2312298

SPIE.

Event: SPIE Astronomical Telescopes + Instrumentation, 2018, Austin, Texas, United States

Testing of a germanium immersion grating

Matthew J. Richter^a, Peter T. Zell^b, Jeffrey S. Logan^b, Robert E. McMurray^b, Curtis N DeWitt^c, Karl W. Kaess^a, Isaiah B. Santistevan^a, Edward J. Montiel^a, Adwin Boogert^d, Thomas P. Greene^b, Scott A. Sandford^b, Takashi Sukagawa^e, and Paul J. Kuzmenko^f

^aUniv of California Davis, 1 Shields Ave, Davis, CA, USA

^bNASA Ames Research Center, Moffett Field, CA, USA

^bSOFIA-USRA, NASA Ames Research Center, Moffett Field, USA

^dInstitute for Astronomy, University of Hawaii at Manoa, 2680 Woodlawn Drive, Honolulu, HI USA

^eOptical Products Operation, Canon Inc, 20-2, Kiyohara-Kogyodanchi, Utsunomiya, Tochigi, JAPAN

^fLawrence Livermore National Lab, Livermore, CA

ABSTRACT

Germanium Immersion Gratings (GIGs) may be an important component for a compact, high-resolution spectrograph for the infrared. Germanium's large index of refraction reduces the length of the grating by a factor of four compared to conventional reflection gratings. Germanium transmits light from roughly 2 to 11.5 μm , which includes spectral regions largely unavailable from the ground because of molecules in Earth's atmosphere. This combination makes GIGs a compelling technology for space missions focused on molecules in astrophysical environments. We are beginning testing of a GIG supplied by Canon, Inc., and anticipate eventual detailed testing of the Canon grating and a similar GIG supplied by LLNL. We also discuss potential science observations that demonstrate the significance of high-resolution, infrared spectroscopy from space.

Keywords: immersion gratings, infrared spectroscopy, high-resolution spectroscopy

1. INTRODUCTION

Infrared spectroscopy is recognized as an important tool for the study of astronomical objects. This is particularly true for studying the molecular universe because of the large number of rotation-vibration transitions available, particularly in the 3 to 10 μm range. Because molecules are frequently found in relatively cool environments, high spectral resolution adds to the usefulness of the observations. Unfortunately, observing from the ground in the 3-10 μm region has significant challenges: 1) the thermal background that results in most of the detected photons coming from warm components in the optical path with non-zero emissivity; and 2) molecules in Earth's atmosphere that both absorb light from the target of interest and contribute additional photons and noise. High spectral resolution can mitigate the atmospheric impact by separating astronomical lines of interest from telluric interference, but high spectral resolution also reduces the number of detected photons per resolution element. As a consequence, high signal-to-noise thermal IR observations at high spectral resolution are mostly limited to the brightest objects.

Space infrared telescopes, such as the Infrared Space Observatory and the Spitzer Space Telescope have been revolutionary in terms of IR spectroscopy.^{1,2} The James Webb Space Telescope should continue this trend. Because these telescopes are above Earth's atmosphere, they have unfettered access to the spectrum. Furthermore, these facilities are cooled so that telescope background drops by a factor of 10^6 .³ Consequently, IR space missions enjoy unprecedented sensitivity compared to the ground.

Unfortunately, IR space missions have been mostly unable to incorporate high spectral resolution (here defined as $R \geq 30,000$). This is in part due to the fact that the resolving power of a diffraction grating is given

Further author information: Send correspondence to Matt Richter - mjrichter@ucdavis.edu

by the path length difference between the extreme ends of the beam in waves. Therefore, high resolution at long wavelengths requires long gratings. As a typical echelle grating might have a 2:1 length to width aspect ratio, the long grating also drives the beam area.

A technology recently brought to fruition in astronomical instruments involves immersion gratings.^{4,5} In an immersion grating, the dispersion occurs within a material instead of in air or vacuum, which reduces the required size of the grating. Germanium has a high index of refraction and is transmissive from roughly 2 to 12 μm , which includes portions of the spectrum severely impacted by Earth's molecular lines. This combination makes Germanium Immersion Gratings (GIGs) extremely attractive as a potential for future space-based infrared spectroscopy missions.

We are in the early stages of a project to test GIGs. Our test gratings are produced by Canon, Inc. and LLNL. The gratings have the same basic specifications with minor differences due to manufacturing techniques. The theoretical limit to these gratings is $R \sim 55,000$ at $\lambda = 5 \mu\text{m}$; our goal is to demonstrate resolving power of $R \geq 40,000$ at $\lambda = 5 \mu\text{m}$. This paper includes descriptions of the optical test setup, the results of initial testing of the Canon grating in immersion configuration, and gives an outlook on progress that will be made in the immediate future.

2. GERMANIUM IMMERSION GRATINGS

The ultimate limit to the resolving power of a diffraction grating is the maximum path length difference between extreme rays expressed in waves:

$$R = (2d \tan \theta) / \lambda$$

where d is the beam diameter, θ is the blaze angle, and λ is the wavelength. Consequently, high resolving power at long wavelengths requires a large path length difference. For a given blaze angle, this results in a large beam diameter and the instrument generally increases in volume.

If diffraction occurs in a medium with non-zero index of refraction, the formula above becomes

$$R = (2dn \tan \theta) / \lambda$$

where n is the index of refraction. Because the wavelength of light we care about is reduced in the refractive medium by n , the resolving power is increased (see Figure 1 taken from work by Kuzmenko et al⁶).

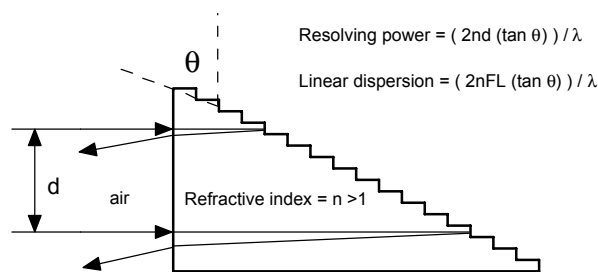


Figure 1. Schematic of an immersion grating with the equations governing resolving power and dispersion. Both quantities are increased by the index of refraction. The figure is taken from Figure 1 of work by Kuzmenko et al.⁶

There are other groups looking at using GIGs in astronomical instruments.^{7,8} The large index, the IR transmission, and the ability to machine germanium as opposed to chemical etching, make it an attractive material.

3. GRATING PRODUCTION

The gratings used for this study both conform to the drawings given in Figures 2 and 3, with minor, non-functional, variations. The 2° wedge at the front face causes light directed perpendicular to the face to be reflected at the surface boundary directly back at the input. Light that enters the crystal and diffracts off the immersion grating will be at an angle of roughly $n \cdot 2 \cdot 2^\circ \approx 16^\circ$ from the input light. The manufacture requires high precision to minimize wavefront error, and in addition to discussing the processes, we examine the magnitudes of the surface irregularities below.

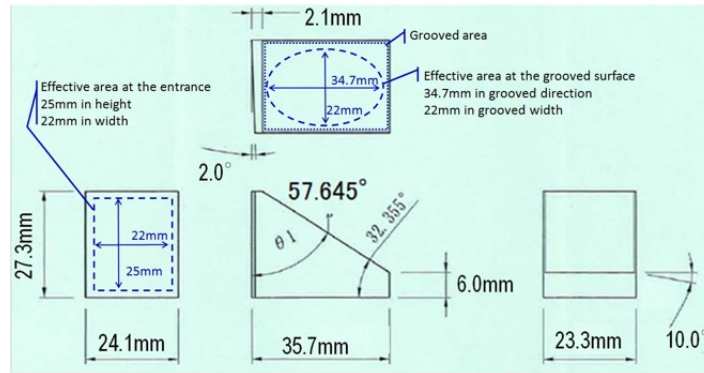


Figure 2. Engineering diagrams of Canon grating

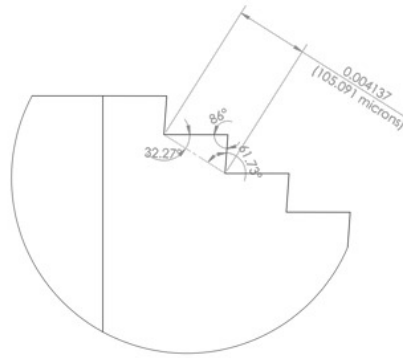


Figure 3. Detailed geometry of Canon GIG groove profile

3.1 LLNL Grating

The process of fabricating a GIG was very similar to that previously reported for other germanium gratings⁶ and grisms⁹ at LLNL. Three blanks of single crystal germanium were purchased from Lattice Semiconductor. The blanks are right angle prisms with rectangular wings parallel to and 0.17 inches below the hypotenuse. These wings support the blank during machining. The 2 cm x 2 cm entrance face is tilted 2 degrees around the vertical axis so that any reflections from the front surface will be directed away from the diffracted beam. Chardon Tool supplied two single crystal diamond tools with a specified blaze angle of 61.7° and a dead sharp tip with an apex angle of 86° . We tested the tools by cutting 8 mm of grooves, with a period $109.735 \mu\text{m}$, in a 25.4 mm diameter, 5 mm thick germanium window that had been acid etched. Microscope inspection showed the grooves to be very clean and free from chipping.

After inspection the blanks were acid etched for several minutes. This removed outer layers of germanium that incurred subsurface damage during fabrication. Pristine crystal is now exposed and the blank is very smooth and shiny. Next the entrance face was polished flat to $\lambda/10$ P-V in the LLNL optics shop.

A program was written to numerically control PERL (the Precision Engineering Research Lathe at LLNL) to machine the GIG. Tool motion along the groove is unidirectional and implements climb cutting as that yields the best results with minimal periodic error. The blank is secured into the machining fixture at three support points on the crystal wings with cyanoacrylate adhesive. The fixture was then installed in PERL, leveled, and squared up with the machine axes to within $1\ \mu\text{m}$, over the length of the blank.

We set the spindle to 1000 rpm and directed a fine spray of light mineral oil over the part. The machine was held in this condition for 20 hours to reach thermal equilibrium before motion of the machine axes was started. The feed rate was 0.35 inches per minute cutting a groove and 2.1 inches per minute moving around the blank to begin the next groove. Machining was completed in around 27 hours (see Figure 4). The barometric pressure was very stable, drifting only 3 mbar over the duration of the cut.

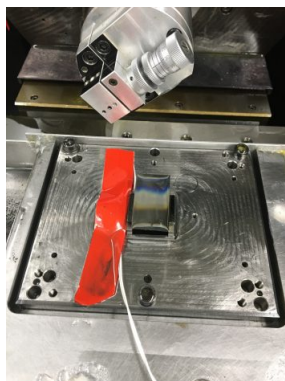


Figure 4. GIGI grating fixtured on PERL at completion of machining

The grating was taken off the machine, flushed with acetone and isopropanol to clean off the mineral oil, and then dried with clean nitrogen. First Contact from Photonic Cleaning Solutions was used to remove residual germanium particles in the grooves. Once cleaned the grooves were inspected under high power magnification (see Figure 5). The groove tops were clean and sharp. Surface figure was measured on a Zygo interferometer viewing the 61.7° grooves. The measured surface error was 0.024 waves rms at 633 nm (see Figure 6).



Figure 5. Section near middle of GIGI grating at 100x magnification shows excellent groove quality

3.2 Canon Grating

Manufacture of the Canon, Inc GIG follows previous descriptions of Canon's capabilities.¹⁰ Canon also uses a cutting process on Germanium. One difference between LLNL and Canon, Inc fabrication is how the crystals are held during cutting. Canon, Inc requires the crystal have extra material, a "pedestal", instead of the wings required by LLNL. For our grating, the pedestal is 6.0 mm high.

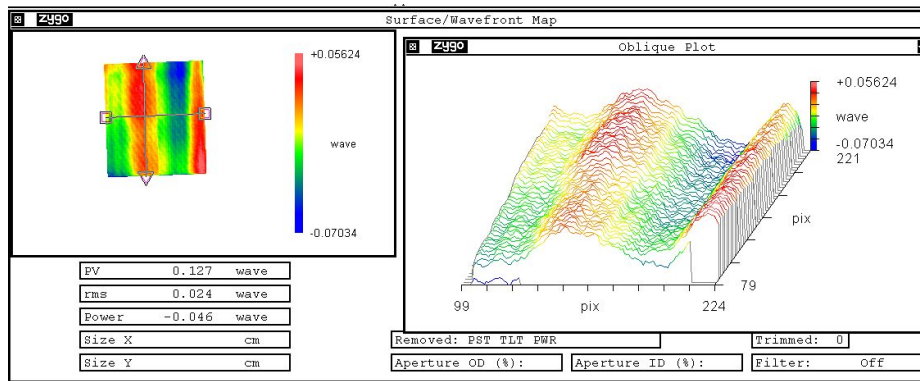


Figure 6. Zygo interferogram of the LLNL grating, showing 0.024 wave surface figure error at 633 nm from 61.7° blazed facets

Following production, a Zygo interferometric measurement of the irregularity of the grating surface was performed, as shown in Figure 7. The Zygo measurement of the Canon, Inc grating shows excellent groove quality with rms of 4.155 nm at 633 nm or 0.0066 wave.

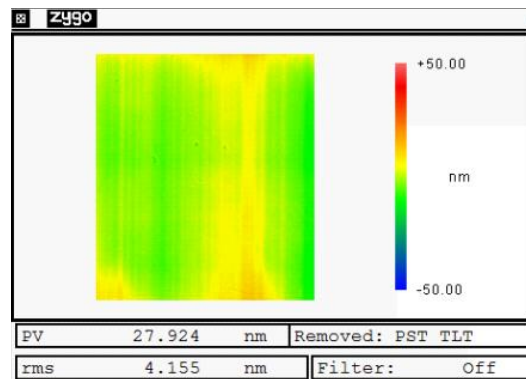


Figure 7. Zygo interferogram provided by Canon, Inc of the GIG we purchased. The groove quality is excellent with rms of 4.155 nm at 633 nm or 0.006 wave.

4. EXPERIMENT

For the initial testing phase, a 3.39 μm laser, the grating and a Teledyne HIRG detector were placed in an optical setup as shown in Figure 8. The detector was placed in an LN-cooled Dewar containing a narrow-band filter and two neutral density filters (not shown). The filtering is required to reduce the background and laser light to acceptable levels for the detector. The upstream optics were spaced to create an expanded, collimated beam that impinged on the grating face at a perpendicular angle. The folding mirror and downstream optics were specified to bring the diffraction lines to a focus at the detector, with the lenses on a translation stage for fine adjustment. The spacing between the grating and the downstream optics lead to spacing between the orders of approximately 21mm, based on optical modeling in Zemax. This spacing does not allow multiple spots to be imaged at the same time on an HIRG, but multiple diffraction spots were observed by taking images at different vertical positions. This technique also allowed establishing the dispersion direction for this setup: -0.3° with respect to the detector vertical.

As a comparison to the grating, a front-surface mirror was used as a stand-in, angled so the beam exiting the mirror would hit the fold mirror shown in the setup (Figure 8) at the same angle as the exiting diffracted light from the grating. This spot was used as a template to adjust the focus of the downstream optics with respect to

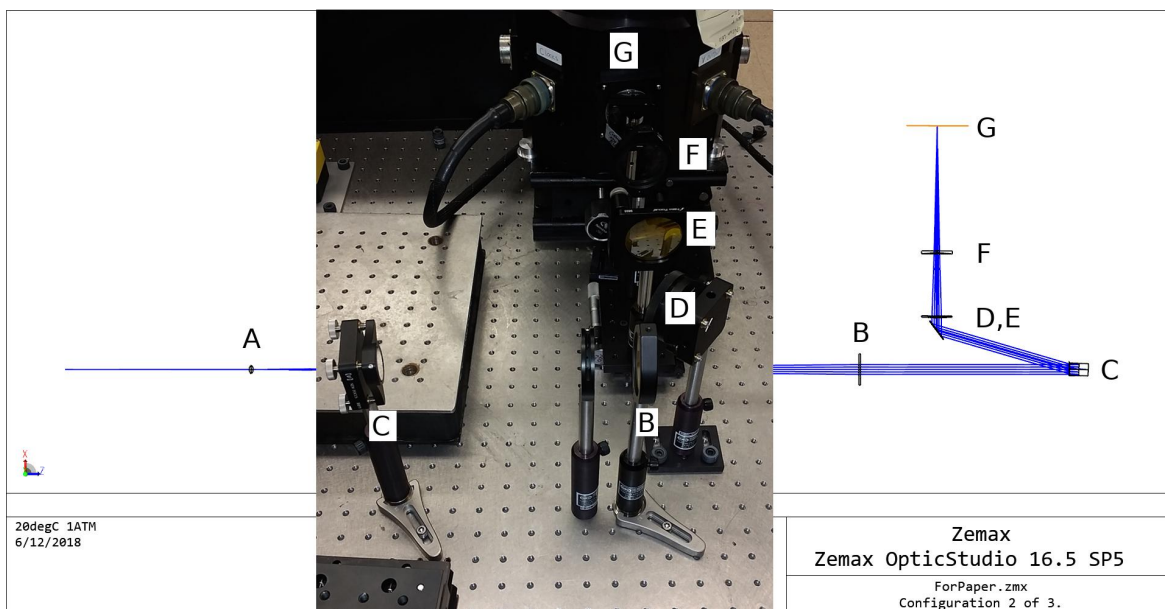


Figure 8. Simplified schematic of optical table. A: Convex lens, B: Collimating Lens, C: Germanium Immersion Grating, D: 2"-gold front-plated mirror, E: Concave Lens, F: Convex Lens, G: HIRG Detector)

the detector plane. The mirror will also serve as a comparison for the efficiency and performance of the grating. With this configuration, images of the spot were taken with multiple non-destructive reads of the HIRG array. The mirror was replaced with the grating, and images of the resulting spot were taken similarly.

Mirror and grating images were analyzed visually, and observed to consist of multiple spot images, both in small clusters and spatially separated. We believe these stray reflections are most likely caused by internal reflections between neutral-density filters. There was sufficient separation between the clusters that the direct image could be isolated and analyzed, and the remaining spots ignored. The clusters consisted of a strong central peak and two smaller side-lobes. These three features were fit using a multiple-2D-Gaussian fit for both the mirror and grating images, and the width of the central peaks analyzed.

In order to isolate the spots from the background, frames were selected from sets of up-the-ramp sequences that maximized signal-to-noise while minimizing saturation/de-biasing. Similar sequences were taken with the laser blocked, and the corresponding frame was used from those sequences to perform background subtraction. The resulting subtracted images were used to perform the fitting as described previously.

In order to visualize the spot-widths, we integrated the images perpendicularly to the dispersion direction along with their corresponding fits, and normalized the resulting profiles. This comparison is shown in Section 5, below.

5. RESULTS

Figure 9 shows the mirror and grating spots after background subtraction juxtaposed with corresponding Gaussian fits. Figure 10 shows the normalized spot profiles along the dispersion direction. From the fit data, the width of the central spot was measured as $1.4x$ the width of the mirror data. However, due to significant and imperfectly-modeled mixing with secondary images, these results should be considered preliminary.

Further work to limit the amount of stray light incident on the detector has already been completed, and allows more frames to be collected in non-destructive reads prior to de-biasing. This and limiting the upstream laser power will allow future analysis to better constrain the pixel values and uncertainties, following, e.g., Rauscher et al.¹¹

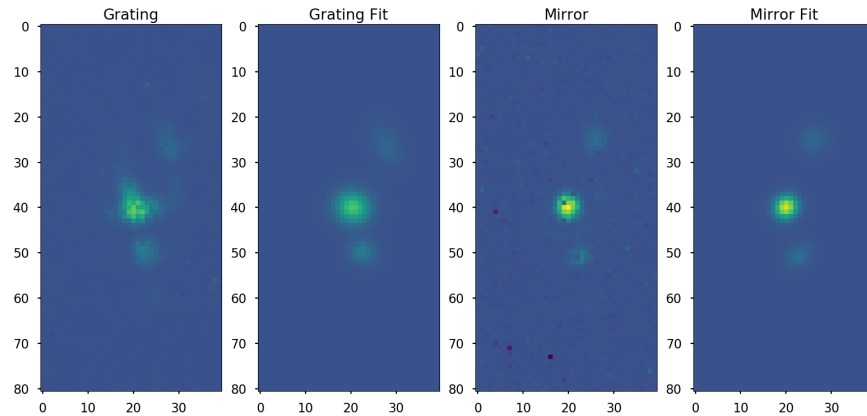


Figure 9. Comparison of grating spots(diffraction) and mirror spots(reflection) juxtaposed with multi-2D-Gaussian fits.

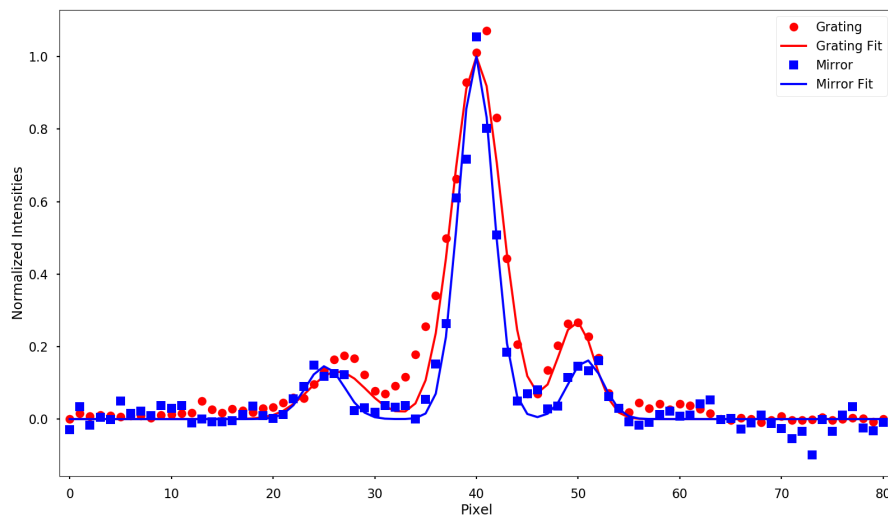


Figure 10. Profiles of grating and mirror spots in dispersion direction with fits, normalize to fit peaks.

Image analysis following the work to reduce stray light, which involved adjustment of the neutral density filters, shows secondary spots at significantly different locations than presented here. In addition to confirming the cause, this may also allow improved isolation of the true spot image and better constraints on the spot profiles.

Immediate follow-up work includes continuing to refine the optical test setup, conduct temperature-controlled warm (room temperature) and cold measurements of the grating after mounting in a Dewar. We anticipate receipt of the LLNL grating during our testing of the Canon grating; we will run the same set of tests on the LLNL grating. After both GIGs have been tested at cryogenic temperatures, we will have them anti-reflection coated by a company to be determined. We will characterize the performance of the GIGs after applying the coating. In

parallel to the optical lab testing, we will be comparing our results to theoretical models of grating performance.

6. SCIENCE GOALS

We identify here some potential applications for a space-based, high spectral resolution instrument featuring a GIG. Detailed consideration of science goals and ensuing instrument requirements will be necessary to bring the project to fruition. Common factors are an emphasis on high spectral resolution of molecular features at wavelengths mostly unavailable from the ground (Figure 11).

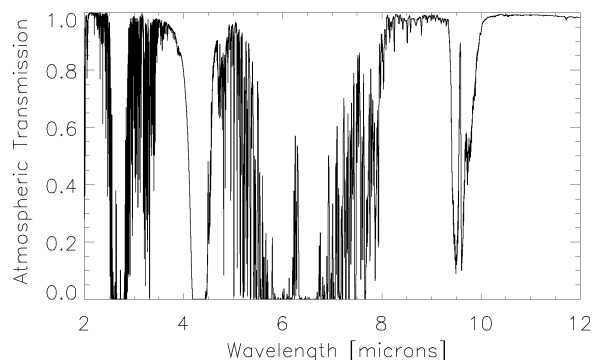


Figure 11. A model of atmospheric transmission from Mauna Kea over the approximate range of transmission for Germanium.

6.1 Astrochemistry

High-resolution, infrared spectroscopy is well suited to studying molecules near sites of recent star formation. The energy from the newly formed star evaporates some of the icy grain mantles in the surrounding cloud. These mantles are rich in simple hydrogenated and oxidized species (e.g., H_2O , CH_4 , NH_3 , CH_3OH , CO , and CO_2 ¹²), and presumably also more complex species. Some important symmetric molecules (CH_4 , CO_2 , C_2H_2), key to the formation of more complex molecules, are available for study in the 3-8 micron region. The warmed dust close to the star becomes a background lamp against which the intervening gas along the line-of-sight will absorb light. The absorption spectra then sample the pencil beam set by the dust continuum. With high-resolution and high signal-to-noise, we would be able to examine the bulk motion of the material through the line profiles as well as determine molecular abundances and gas temperatures. are formed in the dense cloud and protostellar collapse phase. Sublimation in the inner protostellar regions creates “hot cores” rich in complex molecules.

6.2 Protoplanetary Systems

Because of surrounding dust, studying the development of protoplanets is best done at long wavelengths (IR and longer) where dust extinction is reduced. With high-resolution IR spectroscopy, it becomes possible to study small spatial scales using the velocity information in the line profiles. At 1 AU from a solar mass star, the orbital velocity is 30 km/s, which is easily resolvable at high resolution.

Observations of CO ro-vibrational transitions near $4.7 \mu\text{m}$ illustrate the usefulness of high resolution studies of protoplanetary disks. Although the atmosphere limits these observations, they have provided unique information about circumstellar disks and planet formation zones. For example, the CO emission line profiles and intensities trace thermally excited gas in Keplerian rotation in the warm, dense inner disk and surface regions.¹³ The inner CO radius increases (0.02-1 AU) at higher luminosities. Establishing the abundances and distributions of other species, inaccessible to ground-based telescopes at sufficient high quality (CH_4 , H_2O , CO_2) in these inner disk regions, bears on the composition of planetary atmospheres that are assembled from the inner disk gas.¹⁴

Ground-based observations of species other than CO have not been possible (e.g., CH_4 , CO_2 , HDO , H_3^+) or only at low sensitivity (e.g., H_2O). H_2O is a critical species in star and planet formation, due to its high abundance

and its role in planetary atmospheres and the emergence of life. The 3-8 μm region contains thousands of H₂O transitions, both ro-vibrational and purely rotational. The highest energy transitions are least obscured by the Earth's atmosphere, and have revealed abundant H₂O in the inner tenths of AU, and are well mixed with CO.^{15,16} Even on the largest ground-based telescopes, however, signal-to-noise values are low, and spectro-astrometric measurements are not possible. A tentatively high value of the ortho over para H₂O abundance ratio implies formation of H₂O under warm conditions, and would exclude an origin in sublimated ices formed during the molecular cloud phase. Space based observations would also give access to species that cannot be observed at other wavelengths due to their low dipole moments, such as CH₄.

6.3 Extra-Solar Planetary Atmospheric

High spectral resolution, infrared observations have recently been used to study the atmospheres of extrasolar planets.¹⁷ With sufficient resolution, it becomes possible to use the radial velocity variations of the planet to isolate molecular spectral features from the planet. This procedure is most effective for hot Jupiters as these systems have the largest velocity variations, but does not require a transiting system. Birkby et al are able to identify the presence of water vapor in the atmosphere of HD 189733b.¹⁷ Other information available with these observations include the planets temperature/ pressure profile, the volume mixing ratios of molecular species, and the orbital velocity (which leads to the inclination of the system). The analysis becomes more robust with increased spectral resolution and with more lines observed. With a space-based instrument, stronger lines of H₂O, CO₂, and CH₄ become available to better study those molecules.

6.4 Solar System Objects

High-resolution ground-based 2-11 μm spectroscopy of comets has led to the detection of many species by their fluorescent emission lines: H₂O, HDO, CO, HCN, CH₄, CH₃D, H₂CO, C₂H₆, NH₃, NH₂, and more (e.g., Mumma & Charnley (2011)¹⁸). The cometary lines are intrinsically very narrow, less than 1 km/s, and thus their detectability increases strongly at higher spectral resolving power. Ground-based observations of CO₂ are not possible, and currently the only space based observations of cometary CO₂ are done at a resolving power of just 50,¹⁹ making abundance estimates uncertain. Nevertheless, CO₂ is likely as abundant as CO in comets, although the abundances are not accurate enough to distinguish between different classes of comets (e.g., organics enriched), which relates to their formation location. The uncertainties also hamper comparisons with interstellar ices studies,¹² e.g., an understanding of the suspected low carbon content of comets with respect to the ISM.

High-resolution infrared spectroscopy is also a proven technique to probe the composition of planetary atmospheres. Contamination by telluric absorption, and thus the need to observe at high Doppler velocities, limits in particular studies of temporal variability. The HDO/H₂O ratio in the Martian atmosphere, for example, traces the origin of water as a result of slight variations in the sublimation and condensation of HDO versus H₂O.^{20,21} Mapping of this ratio during different Martian seasons is thus needed to constrain the origin of Mars' water. Similarly, mapping of CH₄ and monitoring it over time may yield the origin (e.g., geological, biological) of this trace species in the Martian atmosphere.

7. CONCLUSION

We have begun testing of germanium immersion gratings. The large index of germanium enables high spectral resolution with a diffraction grating significantly smaller than conventional gratings. The transmission of germanium includes regions of the spectrum where ground-based observations are essentially impossible. This combination of reducing the size of a GIG-based spectrograph and the transmission region, make GIGs a potential key technology for the first space-based, high-resolution, IR spectrograph. We have acquired one grating from Canon, Inc and expect to receive a grating from LLNL soon. While our optical test setup needs further refinement before we can draw conclusions, we have been able to use the Canon, Inc grating in conjunction with a 3.39 μm laser. We believe that a successful GIG-based spectrograph would advance our understanding of a variety of astrophysical objects where molecules are important.

ACKNOWLEDGMENTS

This work has been funded by NASA Ames CIF awards in 2016 and 2017. It is also supported by NASA APRA grant NNX17AE70G.

REFERENCES

- [1] van Dishoeck, E. F., “ISO Spectroscopy of Gas and Dust: From Molecular Clouds to Protoplanetary Disks,” *ARA&A* **42**, 119–167 (Sept. 2004).
- [2] Carr, J. S. and Najita, J. R., “Organic Molecules and Water in the Planet Formation Region of Young Circumstellar Disks,” *Science* **319**, 1504 (Mar. 2008).
- [3] Tokunaga, A. T., [*Infrared Astronomy*], 143 (2000).
- [4] John Rayner, Tim Bond, M. B. D. J. G. M. A. T., “ishell: a 1-5 micron cross-dispersed $r=70,000$ immersion grating spectrograph for irtf,” (2012).
- [5] Park, C., Jaffe, D. T., Yuk, I.-S., Chun, M.-Y., Pak, S., Kim, K.-M., Pavel, M., Lee, H., Oh, H., Jeong, U., Sim, C. K., Lee, H.-I., Nguyen Le, H. A., Strubhar, J., Gully-Santiago, M., Oh, J. S., Cha, S.-M., Moon, B., Park, K., Brooks, C., Ko, K., Han, J.-Y., Nah, J., Hill, P. C., Lee, S., Barnes, S., Yu, Y. S., Kaplan, K., Mace, G., Kim, H., Lee, J.-J., Hwang, N., and Park, B.-G., “Design and early performance of IGRINS (Immersion Grating Infrared Spectrometer),” in [*Ground-based and Airborne Instrumentation for Astronomy V*], *Proc.SPIE* **9147**, 91471D (July 2014).
- [6] Paul J. Kuzmenko, Pete J. Davis, S. L. L. L. M. L. J. V. B., “High efficiency germanium immersion gratings,” (2006).
- [7] Yuki Sarugaku, Yuji Ikeda, S. K. N. K. T. S. T. A. S. K. K. N. C. Y. H. K., “Cryogenic performance of high-efficiency germanium immersion grating,” (2016).
- [8] Ikeda, Y., Kobayashi, N., Sarugaku, Y., Sukegawa, T., Sugiyama, S., Kaji, S., Nakanishi, K., Kondo, S., Yasui, C., Kataza, H., Nakagawa, T., and Kawakita, H., “Machined immersion grating with theoretically predicted diffraction efficiency,” *Appl. Opt.* **54**, 5193–5202 (Jun 2015).
- [9] Paul J. Kuzmenko, Steve L. Little, L. M. L. J. C. W. M. F. S. P. M. H. J. M. L. O. D., “Fabrication and testing of germanium grisms for Imircam,” (2012).
- [10] Takashi Sukegawa, Takeshi Suzuki, T. K., “Astronomical large ge immersion grating by canon,” (2016).
- [11] Rauscher, B., Fox, O., Ferruit, P., Hill, R., Waczynski, A., Wen, Y., XiaSerafino, W., Mott, B., Alexander, D., Brambora, C., Derro, R., Engler, C., Garrison, M., Johnson, T., Manthripragada, S., Marsh, J., Marshall, C., Martineau, R., Shakoorzadeh, K., Wilson, D., Roher, W., Smith, M., Cabelli, C., Garnett, J., Loose, M., WongAnglin, S., Zandian, M., Cheng, E., Ellis, T., Howe, B., Jurado, M., Lee, G., Nieznanski, J., Wallis, P., York, J., Regan, M., Hall, D., Hodapp, K., Bker, T., DeMarchi, G., Jakobsen, P., and Strada, P., “Detectors for the *James Webb Space Telescope* nearinfrared spectrograph. i. readout mode, noise model, and calibration considerations,” *Publications of the Astronomical Society of the Pacific* **119**(857), 768–786 (2007).
- [12] Boogert, A. A., Gerakines, P. A., and Whittet, D. C., “Observations of the icy universe,” *Annual Review of Astronomy and Astrophysics* **53**(1), 541–581 (2015).
- [13] Blake, G. A. and Boogert, A. C. A., “High-Resolution 4.7 Micron Keck/NIRSPEC Spectroscopy of the CO Emission from the Disks Surrounding Herbig Ae Stars,” *ApJL* **606**, L73–L76 (May 2004).
- [14] Öberg, K. I., Murray-Clay, R., and Bergin, E. A., “The Effects of Snowlines on C/O in Planetary Atmospheres,” *ApJL* **743**, L16 (Dec. 2011).
- [15] Pontoppidan, K. M., Salyk, C., Blake, G. A., and Käufel, H. U., “Spectrally Resolved Pure Rotational Lines of Water in Protoplanetary Disks,” *ApJ* **722**, L173–L177 (Oct. 2010).
- [16] Salyk, C., Lacy, J. H., Richter, M. J., Zhang, K., Blake, G. A., and Pontoppidan, K. M., “Detection of Water Vapor in the Terrestrial Planet Forming Region of a Transition Disk,” *ApJ* **810**, L24 (Sept. 2015).
- [17] Birkby, J. L., de Kok, R. J., Brogi, M., de Mooij, E. J. W., Schwarz, H., Albrecht, S., and Snellen, I. A. G., “Detection of water absorption in the day side atmosphere of HD 189733 b using ground-based high-resolution spectroscopy at $3.2\mu\text{m}$,” *MNRAS* **436**, L35–L39 (Nov. 2013).

- [18] Mumma, M. J. and Charnley, S. B., “The Chemical Composition of Comets—Emerging Taxonomies and Natal Heritage,” *ARA&A* **49**, 471–524 (Sept. 2011).
- [19] Ootsubo, T., Kawakita, H., Hamada, S., Kobayashi, H., Yamaguchi, M., Usui, F., Nakagawa, T., Ueno, M., Ishiguro, M., Sekiguchi, T., Watanabe, J.-i., Sakon, I., Shimonishi, T., and Onaka, T., “AKARI Near-infrared Spectroscopic Survey for CO₂ in 18 Comets,” *ApJ* **752**, 15 (June 2012).
- [20] Encrenaz, T., DeWitt, C., Richter, M. J., Greathouse, T. K., Fouchet, T., Montmessin, F., Lefèvre, F., Forget, F., Bézard, B., Atreya, S. K., Case, M., and Ryde, N., “A map of D/H on Mars in the thermal infrared using EXES aboard SOFIA,” *A&A* **586**, A62 (Feb. 2016).
- [21] Villanueva, G. L., Mumma, M. J., Novak, R. E., Käufl, H. U., Hartogh, P., Encrenaz, T., Tokunaga, A., Khayat, A., and Smith, M. D., “Strong water isotopic anomalies in the martian atmosphere: Probing current and ancient reservoirs,” *Science* **348**, 218–221 (Apr. 2015).